International Journal of ISSI, Vol.1 (2004), No. 1, pp. 1-7

Optimization of Hot Workability in Ti-IF Steel by Using the Processing Map

R. Ebrahimi* and A. Najafizadeh
Department of Materials Engineering, Isfahan University of Technology, Isfahan, 84156, Iran
Received February 28, 2004; accepted June 13, 2004

Abstract
Processing map for hot working of Ti-IF steel has been developed in the temperature range of 750 to 1100 °C and strain rate of 0.01 to 100 s^{-1}. This map in the austenite region exhibits a single domain with a peak efficiency of 45% occurring at 1025 °C and strain rate of 0.02 s^{-1}. The domain extends over the temperature range of 1000 to 1100 °C and strain rate range of 0.01 to 1 s^{-1}. The true stress-strain curves and microstructural observations shows the occurrence of dynamic recrystallization in this domain. In two phase regions, where austenite and ferrite are present together, flow localization occurs in the form of bands with a fine grained structure as a result of dynamic recrystallization in the bands. These deformation bands are formed at 45° with respect to axial direction of compression. The processing map in ferrite region exhibits a domain with a peak efficiency of 38% occurring at 825 °C and strain rate of 0.02 s^{-1}, so this domain extends over the temperature range of 800 to 850 °C and strain rate range of 0.01 to 0.5 s^{-1}. The true stress-strain curves and microstructural results confirm the occurrence of partially dynamic recrystallization in this domain.

Keywords: Hot working, Processing map, Ti-IF steel, Dynamic recrystallization

Introduction

Interstitial free steels are used extensively in the automotive industry. Historically, these steels have evolved from low strength, high ductility types of steel to high strength, and high ductility steels, driven by the necessity of producing thinner gauges for reducing weight, and consequently, energy consumption [1-2]. Therefore investigation on hot deformation behavior of these steels can be benefitial for metallurgical design of hot metal forming processes.

The hot working characteristics of Ti-IF steel have been studied extensively using different techniques. The influence of hot deformation parameters on the hot workability and the development of microstructure have also been reported [3-6]. Although these studies have led to understanding the mechanisms of hot deformation, they cannot be directly used to optimize hot workability. The aim of the present work is to develop a processing map for Ti-IF steel in order to optimize the hot workability and controlling the microstructure.

Dynamic Materials Model

The processing maps are developed on the basis of the principles of the Dynamic Materials Model [7] which has been reviewed by Gegel et al [8].

* *Corresponding author:*
Tel:+98-711-6286531 Fax:+98-711-6287294
E-mail address:Ebrahimi_ramin@yahoo.com
Address:Dept.of Materials Science and Engineering
Shiraz University, Shiraz, IRAN

In this model, the work piece under hot working conditions is considered to be a dissipator of power. At any instant, the power dissipation occurs through a temperature rise (G content) and a microstructural change (J co-content), and the partitioning between these two is decided by the strain rate sensitivity (m) of flow stress (σ). At a constant temperature and strain, the dynamic response of the work piece material undergoing hot deformation is represented by the constitutive equation:

$$\sigma = C\dot{\varepsilon}^m \qquad (1)$$

The strain rate sensitivity (m) is the inverse of the stress exponent (n) in the standard kinetic rate equation describing the hot deformation. The J co-content is given by [7]:

$$J = \int_0^\sigma \dot{\varepsilon} d\sigma = \frac{\sigma \dot{\varepsilon} m}{m+1} \qquad (2)$$

Where σ is the flow stress and $\dot{\varepsilon}$ is the strain rate. For an ideal linear dissipator, m=1 and $J = J_{\max} = \sigma\dot{\varepsilon}/2$. The efficiency of power dissipation of a non-linear dissipator may be expressed as a dimensionless parameter:

$$\eta = \frac{J}{J_{\max}} = \frac{2m}{m+1} \qquad (3)$$

where Eq. (3) indicates η as independent of $\dot{\varepsilon}$. This equation is applicable only if the plot of σ versus $\dot{\varepsilon}$ for a constant T and ε follow the power-law distribution as in Eq. (1). Otherwise, using the slope of the $\ln(\sigma)$-$\ln(\dot{\varepsilon})$ curve for evaluating η is

erroneous. In such a situation, the integral for J can be evaluated from the test data through a cubic spline fit. The advantage of adopting a cubic spline fit is to generate a greater number of data points, which will be useful for evaluating the integrals by trapezoidal rule. Now, the efficiency parameter (η) can be written as

$$\eta = \frac{J}{J_{\max}} = \frac{\int_0^{\sigma} \dot{\varepsilon} d\sigma}{\frac{\sigma\dot{\varepsilon}}{2}} \tag{4}$$

by using Eq.(1) where m is as a function of $\dot{\varepsilon}$ thus the Eq.(4) becomes:

$$\eta = \frac{C\int_0^{\sigma} m\dot{\varepsilon}^m d\dot{\varepsilon}}{C\frac{\dot{\varepsilon}^{m+1}}{2}} \tag{5}$$

Generally, the test data of σ-$\dot{\varepsilon}$ will be generated for $10^{-2} < \dot{\varepsilon} < 10^{2}$, whereas the integration in Eq.(5) for J needs input from $\dot{\varepsilon} = 0$. To overcome this difficulty, the integral for η is split as:

$$\eta = \frac{\left.\frac{m\dot{\varepsilon}^{m+1}}{m+1}\right|_{\dot{\varepsilon}_{\min}} + \int_{\dot{\varepsilon}_{\min}}^{\dot{\varepsilon}} m\dot{\varepsilon}^m d\dot{\varepsilon}}{\frac{\dot{\varepsilon}^{m+1}}{2}} \tag{6}$$

where the value of m at $\dot{\varepsilon}_{\min}$ obtained from the slope of ln(σ)-ln($\dot{\varepsilon}$) curve close to the point, $\dot{\varepsilon} = \dot{\varepsilon}_{\min} = 10^{-2}$. Therefore, the integral in Eq.(6) can be calculated by trapezoidal rule. The variation of η which is usually expressed as percent, with temperature and strain rate, represents the power dissipation characteristics occurring through microstructural changes in the work piece material and constitutes a power dissipation map. This map exhibits different domains, which may be correlated with specific microstructural processes. The maximum efficiency of power dissipation is about 30-35%, 40% and 50-55% for low, medium and high stacking fault energy materials respectively, which may be useful for the interpretation of processing maps. Higher efficiency of power dissipation (>60%) in relation to the superplasticity and wedge cracking may occur in some materials at special conditions [9].

Instability Criterion

The dynamic materials model has as its basis the extremum principles of irreversible thermodynamics as applied to large plastic flow described by Ziegler [10]. Kumar [11] and Prasad [12] have developed a criterion for evaluating the regimes of flow instabilities. The criterion is based on the continuum principles as applied to large plastic flow proposed by Ziegler [10]. According to this criterion the instabilities occur when,

$$\frac{\partial D}{\partial \dot{\varepsilon}} < \frac{D}{\dot{\varepsilon}} \tag{7}$$

where $D(\dot{\varepsilon})$ is the dissipation function at a given temperature. By this criterion $D(\dot{\varepsilon})$ is equivalent to J co-content which represents the power dissipation through microstructural changes, and the above equation is transformed to,

$$\frac{\partial J}{\partial \dot{\varepsilon}} < \frac{J}{\dot{\varepsilon}} \tag{8}$$

Equation (8) can be written in the form,

$$\frac{\partial \ln J}{\partial \ln \dot{\varepsilon}} < 1 \tag{9}$$

Taking logarithms on both sides of Eq. (2),

$$\ln J = \ln\left(\frac{m}{m+1}\right) + \ln\sigma + \ln\dot{\varepsilon} \tag{10}$$

and differentiating Eq. (10) with respect to $\ln\dot{\varepsilon}$ obtains,

$$\frac{\partial \ln J}{\partial \ln \dot{\varepsilon}} = \frac{\partial \ln\left(\frac{m}{m+1}\right)}{\partial \ln \dot{\varepsilon}} + \frac{\partial \ln \sigma}{\partial \ln \dot{\varepsilon}} + 1 \tag{11}$$

Using equations (1) and (9) and (11), the condition for instability is obtained as

$$\xi(\dot{\varepsilon}) = \frac{\partial \ln\left(\frac{m}{m+1}\right)}{\partial \ln \dot{\varepsilon}} + m < 0 \tag{12}$$

It should be noted that, Eq.(2) for J in terms of m, σ, and $\dot{\varepsilon}$ is obtained by assuming the constitutive relation (1) in which m is independent of $\dot{\varepsilon}$. Then Eq.(12) is reduced to $m < 0$ for the metallurgical instability. Hence, the instability condition of Eq.(12) derived by Kumar [11] and used by Prasad [12] is not applicable for any type of σ versus $\dot{\varepsilon}$ curve. A simple condition for the metallurgical instability from Eq.(12) in terms of η and m, is derived and is described as below.

The derivative of J with respect to $\dot{\varepsilon}$ from Eq.(2) can be written as,

$$\frac{\partial J}{\partial \dot{\varepsilon}} = \frac{\partial \sigma}{\partial \dot{\varepsilon}}\dot{\varepsilon} = \sigma\frac{\partial \ln \sigma}{\partial \ln \dot{\varepsilon}} = m\sigma \tag{13}$$

From Eq.(3), the ratio of J to $\dot{\varepsilon}$ can be written in the form,

$$\frac{J}{\dot{\varepsilon}} = \frac{1}{2}\eta\sigma \tag{14}$$

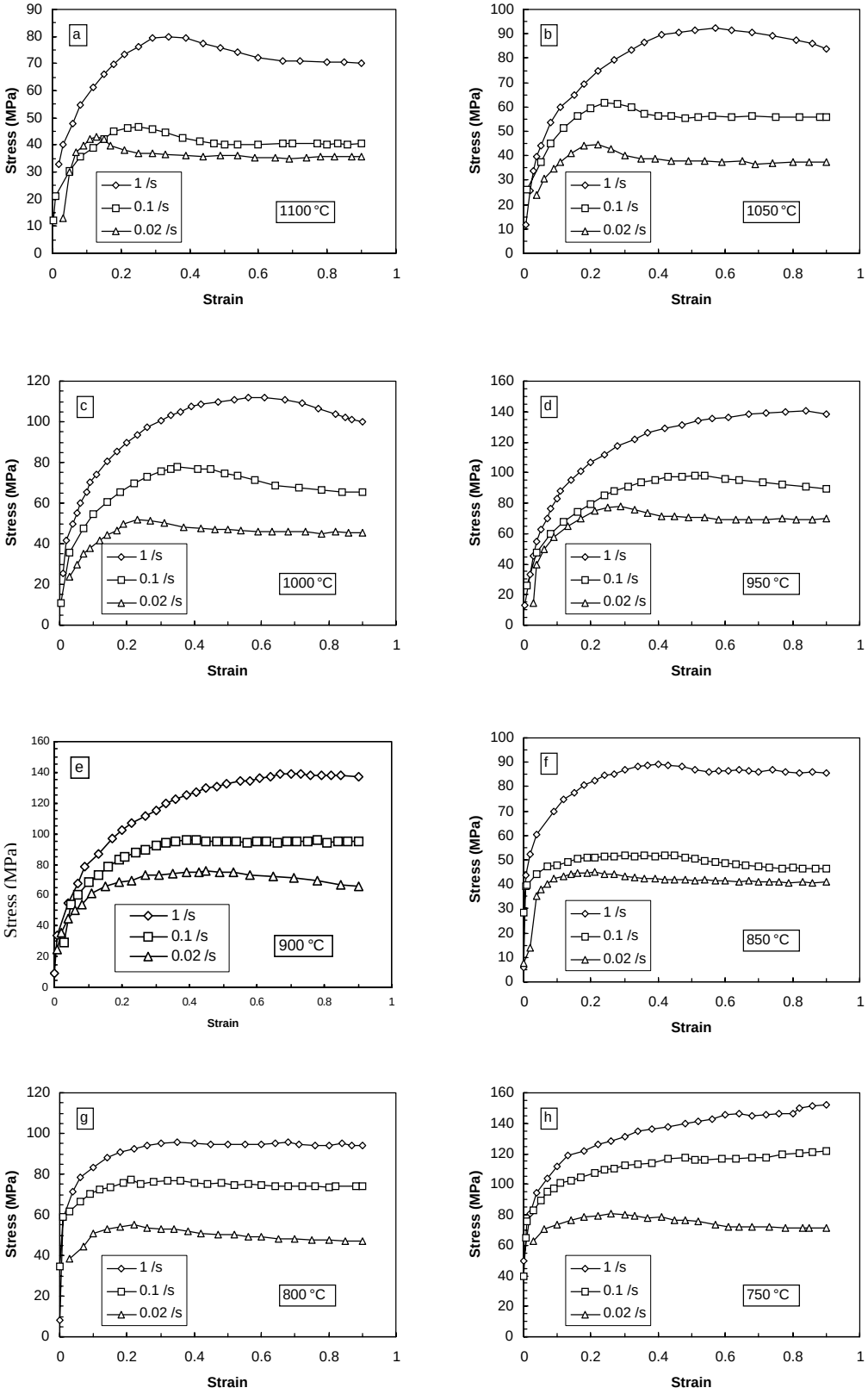

Fig. 1. The true stress-true strain curves in hot compression tests at a temperature range of 750-1100 °C and a strain rate of 0.02, 0.1 and 1 s^{-1} for Ti-IF steel.
a) 1100 °C, b) 1050 °C, c) 1000 °C, d) 950 °C, e) 900 °C, f) 850 °C, g) 800 °C, h) 750 °C

By replacing equations (13) and (14) in Eq.(8), the metallurgical instability condition in terms of η and m, can be written in the form,

$$2m < \eta \qquad (15)$$

Thus, for stable material flow, $\eta < 2m$ and $0 < m < 1$. The instability criterion (Eq.15) is valid for any type of σ versus $\dot{\varepsilon}$ curve. The applicability of this condition has been verified for several materials [13-14].

The variation of the instability parameters $\xi(\dot{\varepsilon})$ and $2m/\eta$ with temperature and strain rate constitutes two instability maps which may be superimposed on the power dissipation map for obtaining a processing map. This methodology has been used to optimize hot workability of a variety of materials [15-18].

Experimental procedure

The chemical composition of the Ti-IF steel used in this investigation is given in table1. The starting material was in the as rolled condition with a initial grain size of 100 μm. The cylindrical hot compression specimens with a diameter of 5 mm and a height of 7.5 mm (Height to diameter ratio of 1.5) were machined from a slab with the deformation axis parallel to hot rolling direction. Concentric grooves, about 0.2mm in depth were engraved on the specimen faces to facilitate the retention of lubricant. A chamfer of 0.5 mm at 45° were machined along the edges of the faces to avoid fold over in the initial stages of the compression. The end faces of the specimens were lubricated with powdered glass. The PtRh10-Pt thermocouple was welded on the surface of cylinder at the mid length of the specimen.

All deformation and dilatometry testing was conducted on a Bähr 805 dilatometer with a deformation unit designed to enable the imposition of a simple uniaxial deformation.

In order to homogenize the specimen before starting the deformation, the cylindrical specimens were heated to 1200°C and holding 5 minutes in an argon atmosphere and then cooled to deformation temperature at which it was held for 1 minute to eliminate the thermal gradient before deformation. Hot compression tests were carried out in the temperature range of 750-1100 °C at intervals 50 °C and in the strain rate of 0.02, 0.1 and 1 s^{-1}.

In order to avoid any microstructural change, the samples were quenched from deformation temperature to room temperature. The cylindrical specimens were then sectioned along their length and examined metallographically.

The procedure for obtaining the power dissipation maps was as follows:

The true stress-strain curves were obtained from load-displacement curves of compression test at constant temperature and true strain rate. The flow stress data at steady state condition as a function of temperature and strain rate were obtained from these curves, then, using usual kinetic model [19], these data extend to large strain rate range of 0.01 to 100 s^{-1} and used to construct the power dissipation maps. The $\ln\sigma$ versus $\ln\dot{\varepsilon}$ data were fitted using a cubic spline and the strain rate sensitivity (m) was calculated as a function of strain rate. This was repeated for various temperatures investigated. The efficiency of power dissipation through microstructural changes was then calculated as a function of temperature and strain rate and plotted as an iso-efficiency map. The values of $\xi(\dot{\varepsilon})$ and $2m/\eta$, given by Eq.(12) and Eq.(6) respectively, were also evaluated and plotted as a function of temperature and strain rate to give two instability maps.

Results and Discussion

Typical true stress-strain curves obtained in the temperature range of 750 to 1100 °C and the strain rate range of 0.02 to 1 s^{-1} are shown in Figure1.

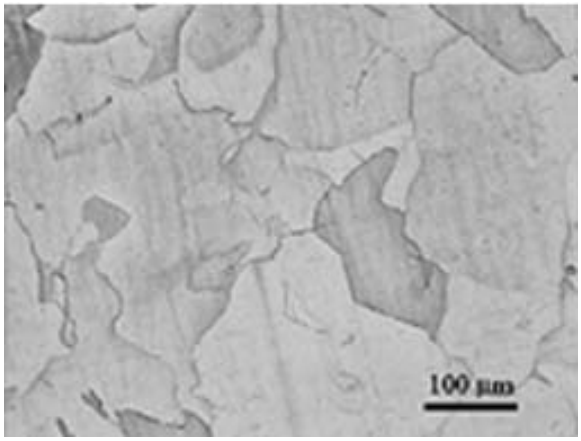

Fig. 2. The microstructure of Ti-IF steel before deformation, heated to the temperature of 1200 °C and holding 5 min. then cooled to deformation temperature of 1000 °C and holding 1 min. and then quenched to room temperature (etching by nital 2%).

Table 1. The chemical composition of Ti-IF steel (wt.%).

C	Si	Mn	P	S	N	Al	Cr	Cu	Mo	Ni	Nb	V	Ti
0.002	0.020	0.13	0.005	0.009	0.0032	0.030	0.037	0.014	0.008	0.025	0.002	0.002	0.062

The shapes of the curves in austenite region above 950 °C at different strain rates show the drop of stress after peak, this is an evidence for the occurrence of dynamic recrystallization. Figure 2 shows the microstructure of specimen before deformation and Figure 3 exhibits the microstructure of specimen after deformation at temperature of 1000 °C and strain rate of 0.1 s^{-1}. The fine and non uniform grains confirmed the occurrence of dynamic recrystallization (Figure 3). In Ferrite region at 850 °C and strain rate of 0.1 s^{-1}, the drop of stress after peak and the microstructural observations (Figure 4) show partially dynamic recrystallization in the ferrite phase. The Ar_1 and Ar_3 temperatures for Ti-IF steel that were obtained from the dilatometry test are 863 and 914 °C, respectively.

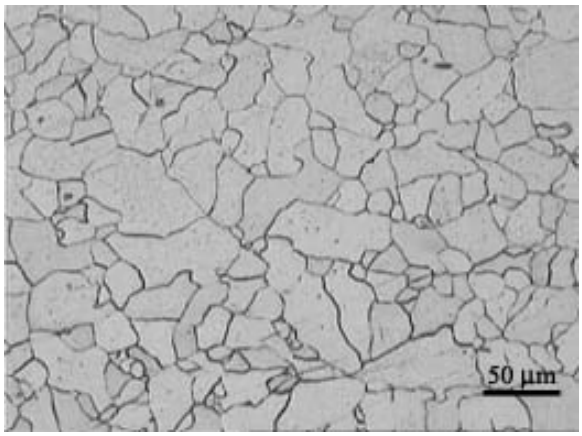

Fig. 3. The microstructure of Ti-IF steel after deformation (ε=0.9) at temperature of 1000 °C and strain rate of 1 s^{-1} (etching by nital 2%).

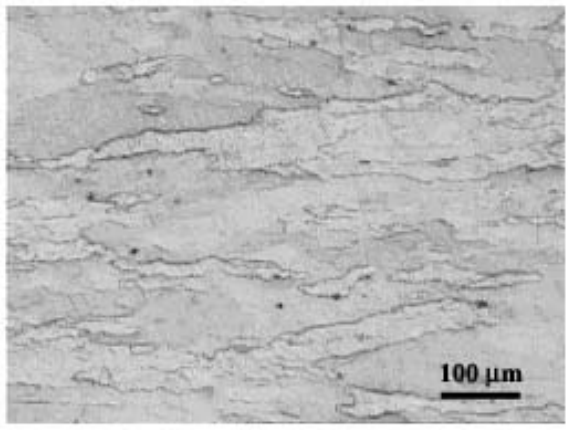

Fig. 4. The microstructure of Ti-IF steel after deformation (ε=0.9) at temperature of 850 °C and strain rate of 0.1 s^{-1} (etching by nital 2%).

The power dissipation map obtained at a strain of 0.9 is presented in Fig.5 which shows the contours of constant efficiency of power dissipation on the temperature-strain rate plane. The maps obtained at other strains at steady state are essentially similar to those shown in Figure 5. this indicates that the effect of strain on the map is not significant. The map in austenite region exhibits a single domain with a peak efficiency of 45% occurring at 1025 °C and strain rate of 0.02 s^{-1} . The domain extends over the temperature range of 1000 to 1100 °C and strain rate range of 0.01 to 1 s^{-1}. The true stress-strain curves and microstructural results showed the occurrence of dynamic recrystallization in this domain. This power dissipation map in ferrite region exhibits a domain with a peak efficiency of 38% occurring at 825 °C and strain rate of 0.02 s^{-1}. So this domain extends over the temperature range of 800 to 850 °C and the strain rate range of 0.01 to 0.5 s^{-1}. The true stress-strain curves and microstructural observations confirmed that partially dynamic recrystallization occurs in this domain.

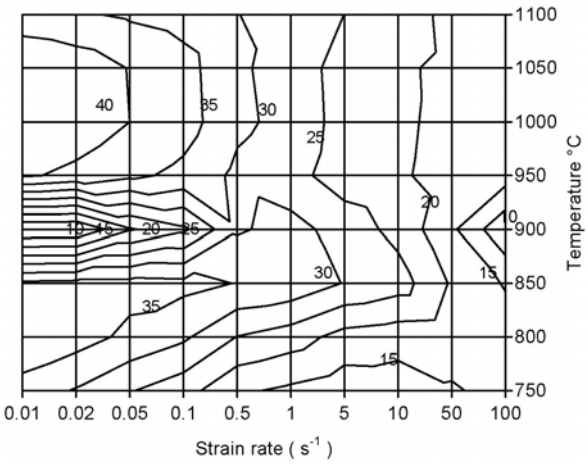

Fig. 5. The power dissipation map obtained at a strain of 0.9 for Ti-IF steel.

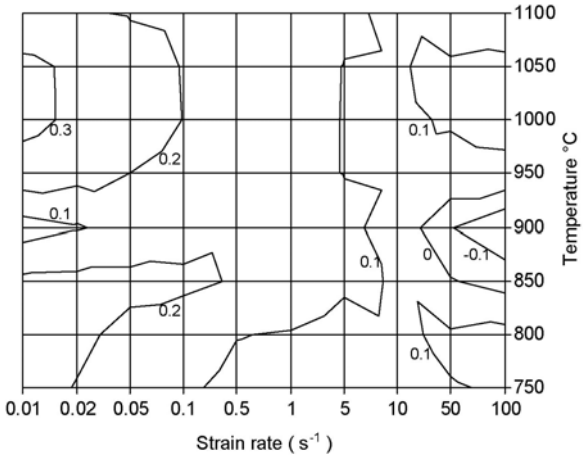

Fig. 6. The instability map according to the parameter $\xi(\dot{\varepsilon})$ at strain of 0.9 for Ti-IF steel.

The instability map showing the contours of $\xi(\dot{\varepsilon})$ on the strain rate-temperature plane is shown in Figure 6. According to the criterion given by Eq.(12), the regime for which $\xi(\dot{\varepsilon})$ is negative will

represent the flow instability. Also, a simple condition for the stable material flow is $\eta/2m < 1$ [20]. Thus according to this criterion, the regime for which $2m/\eta$ is less than unit will represent the flow instability (Figure 7).

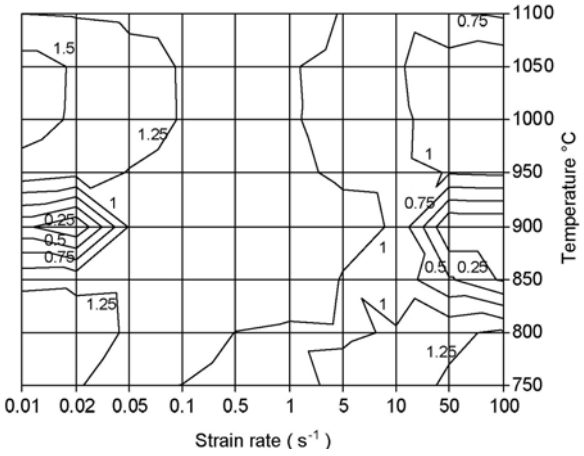

Fig. 7. The instability map according to the parameter $2m/\eta$ at strain of 0.9 for Ti-IF steel.

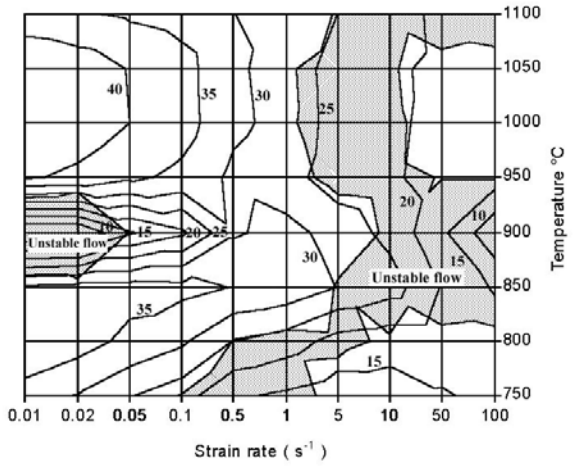

Fig. 8. The processing map for Ti-IF steel at strain of 0.9.

Figure 8 shows the processing maps obtained from superimposing of instability maps on deformation efficiency map of Ti-IF steel. According to the processing map, the material is expected to show flow instability at strain rates of higher than about 1 s^{-1} and lower than 0.05 s^{-1} in the two-phase region. The microstructural features of the instability are shown in Figure 9 which correspond to a strain rate of 0.02 s^{-1} at 900°C. The microstructure shows a flow localization in the form of deformation bands with a fine grained structure formed as a result of dynamic recrystallization in bands. These bands are formed at 45° with respect to axial direction of compression. These bands correspond to narrow regions of intense shear that occur independent of the grain structure and also, of normal crystallographic considerations. Therefore, the strain at these bands reach critical strain for the start of dynamic recrystallization thus, which occurs in deformation bands locally and induces very small grains size (<2μm). In two-phase region, deformation enhanced transformation, referring to the transformation of austenite to ferrite under conditions of straining [21].

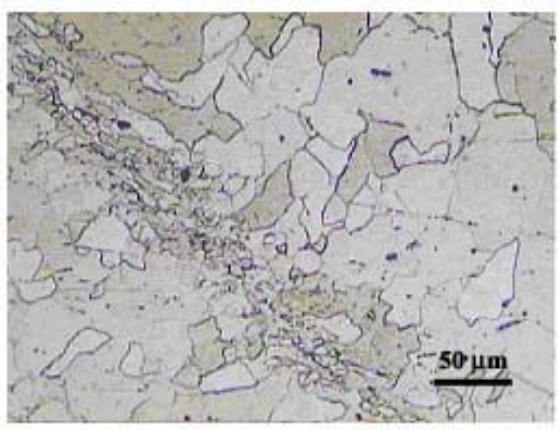

Fig. 9. The microstruture of Ti-IF steel after deformation (ε=0.9) at temperature of 900 °C and strain rate of 0.02 s^{-1} (etching by nital 2%).

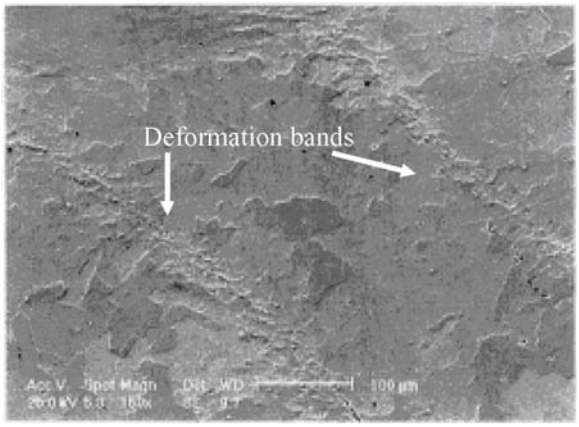

Fig. 10. The SEM micrograph of Ti-IF steel after deformation (ε=0.9) at temperature of 900 °C and strain rate of 0.02 s^{-1} (etching by nital 2%).

The driving force of the transformation, as well as the nucleation rate, will be significantly increased under this condition. These phenomena, cause more ferrite phase to form at 45° direction since ferrite is softer than austenite. When these two phases are present together at the same temperature, then localization occurs in this region that has maximum shear stress due to the geometry of specimen. The SEM micrograph of this specimen exhibits two parallel deformation bands (Figure 10). Figure 11 shows the geometry of the specimen after deformation at 900 °C with strain rate of 0.02 s^{-1} that flow localization leads to this shape.

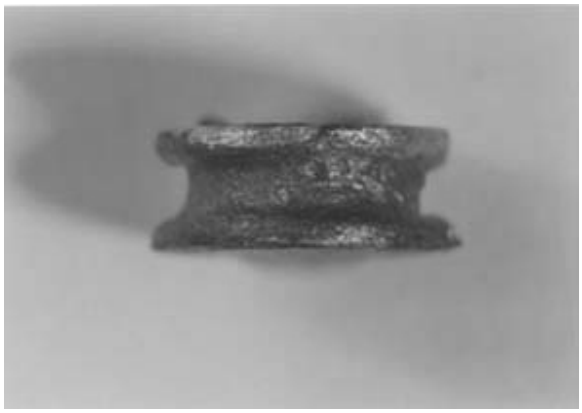

Fig. 11. The geometry of specimen after deformation (ε=0.9) at temperature of 900 °C and strain rate of 0.02 s^{-1}.

Conclusion

1- The dilatometry test showed that the Ar_1 and Ar_3 temperatures for Ti-IF steel are 863 and 914°C ,respectively.

2- The processing map in the austenite region exhibits a single domain with a peak efficiency of 45% occurring at 1025 °C and strain rate of 0.02 s^{-1} . The domain extends over the temperature range of 1000 to 1100 °C and strain rate range of 0.01 to 1 s^{-1}.

3- According to the processing map, the material is expected to show flow instability at strain rates of higher than about 1 s^{-1} and lower than 0.05 s^{-1} in the two-phase region.

4- In the two phase region which corresponds to a strain rate of 0.02 s^{-1} at 900°C, the microstructure shows flow localization in the form of deformation bands with a fine grained structure formed as a result of dynamic recrystallization in such bands. These bands are formed at 45° with respect to axial direction of compression.

5- The processing map in ferrite region exhibits a domain with a peak efficiency of 38% occurring at 825 °C and strain rate of 0.02 s^{-1}. This domain extends over the temperature range of 800 to 850 °C and strain rate range of 0.01 to 0.5 s^{-1}.

References

[1] H. Takechi, IF Steels 2000 Proceedings, (2000),1.
[2] T. Senuma, ISIJ Int., 41(2001), 520.
[3] A. Najafizadeh, J. J. Jonas, and S. Yue, Met. Trans. 23A(1992), 2607.
[4] M. R. Barnett and J. J. Jonas, ISIJ Int., 39(1999), 856.
[5] B. Hutchinson and D. Artymowicz, ISIJ Int., 41(2001), 533.
[6] C. J. Barrett and B. Wilshire, J. Mater. Processing Tech., 122(2002), 56.
[7] Y. V. R. K. Prasad, H. L. Gegel, S. M. Doraivelu, J. C. Malas, J. T. Morgan, K. A. Lark, and D. R. Barker, Metall. Trans. A, 15(1984), 1883.
[8] H. L. Gegel, J. C. Malas, S. M. Doraivelu, and V. A. Shende,: Metals Handbook Vol.14 , ASM, Metals Park, Ohio, (1987), 417.
[9] Y. V. R. K. Prasad and T. Seshacharyulu, Int. Mater. Rev.,43(1998), 243.
[10] H. Ziegler :Progress in Solid Mechanics, Vol.4, Wiley, New York, (1963), 93.
[11] A. K. S. Kalyan Kumar, "Criteria for Predicting Metallurgical Instabilities in Processing Maps", M.Sc Thesis, Indian Institute of Science, Bangalore, India, 1987.
[12] Y. V. R. K. Prasad, Indian J. Tech., 28(1990), 435.
[13] S. V. S. Narayana Murty and B. Nageswara Rao, J. Mater. Sci Lett., 17(1998), 1203.
[14] S. V. S. Narayana Murty and B. Nageswara Rao, Mater. Sci. and Eng. A ,245(1998), 76.
[15] J. K. Chakravaritty, Y. V. R. K. Prasad, and M. K. Asundi, Metall. Trans. A22 (1991), 829.
[16] O. Sivakesavam, I. S. Rao, and Y. V. R. K. Prasad, Mater. Sci. Tech.,9(1993), 805.
[17] B. V. Radhakrishna Bhat, Y. R. Mahajan, and Y. V. R. K. Prasad, Metall. Mater. Trans., 31 A(2000), 629.
[18] P. V. Sivaprasad, S. Venugopal, Sridhar Venugopal, V. Maduraimuthu, M. Vasudevan, S. L. Mannan, Y. V. R. K. Prasad, and R. C. Chaturvedi, J. Mater. Processing Tech., 132(2003), 262.
[19] G. Krauss, Deformation of Materials, ASM, Metals Park, Ohio, (1985), 113.
[20]. S. V. S. Narayana Murty, B. Nageswara Rao, and B. P. Kashyap, Int. Mater. Rev., 45(2000),15.
[21] D. N. Hanlon, J. Sietsma, and S. van der Zwaag, ISIJ Int., 41(2001), 1028.